

UC Irvine

UC Irvine Previously Published Works

Title

Alternative cell polarity behaviours arise from changes in G-protein spatial dynamics

Permalink

<https://escholarship.org/uc/item/8vj1b7pk>

Journal

IET Systems Biology, 9(2)

ISSN

1751-8849

Authors

Chou, Ching-Shan

Moore, Travis I

Nie, Qing

et al.

Publication Date

2015-04-01

DOI

10.1049/iet-syb.2013.0018

Peer reviewed



Alternative cell polarity behaviours arise from changes in G-protein spatial dynamics

Ching-Shan Chou^{1*}, Travis I. Moore^{2*}, Qing Nie³, Tau-Mu Yi⁴

¹Department of Mathematics, The Ohio State University, Columbus, OH 43210, USA

²Department of Biological Chemistry and Molecular Pharmacology, Program in Cellular and Molecular Medicine, Boston Children's Hospital, Harvard Medical School, Boston, MA 02115, USA

³Department of Mathematics, University of California, Irvine, CA 92697, USA

⁴Molecular, Cellular, and Developmental Biology, 1111 Biological Sciences II, University of California, Santa Barbara, CA 93106, USA

*Co-first authors

E-mail: taumu.yi@lifesci.ucsb.edu

Abstract: Yeast cells form a single mating projection when exposed to mating pheromone, a classic example of cell polarity. Prolonged treatment with pheromone or specific mutations results in alternative cell polarity behaviours. The authors performed mathematical modelling to investigate these unusual cell morphologies from the perspective of balancing spatial amplification (i.e. positive feedback that localises components) with spatial tracking (i.e. negative feedback that allows sensing of gradient). First, they used generic models of cell polarity to explore different cell polarity behaviours that arose from changes in the model spatial dynamics. By exploring the positive and negative feedback loops in each stage of a two-stage model, they simulated a variety of cell morphologies including single bending projections, single straight projections, periodic multiple projections and simultaneous double projections. In the second half of the study, they used a two-stage mechanistic model of yeast cell polarity focusing on G-protein signalling to integrate the modelling results more closely with the authors' previously published experimental observations. In summary, the combination of modelling and experiments describes how yeast cells exhibit a diversity of cell morphologies arising from two-stage G-protein signalling dynamics modulated by positive and negative feedbacks.

1 Introduction

Cell polarity arises from the breaking of symmetry in response to an internal or external cue [1]. From this asymmetry, the complexity of cellular form and function arises. These cues can change in time and space and are monitored by the organism. One type of extracellular signal is a chemical gradient; cells polarise by making a projection or moving with respect to the gradient direction. Examples of gradient-sensing behaviour include neutrophil and macrophage migration, neuronal axon guidance, slime mold aggregation and yeast mating projection formation [2–5].

Proper cell polarity positions components to the front (or back) of the cell, and such tight localisation often requires amplification provided by positive feedback [6, 7]. On the other hand, this internal spatial pattern must have the ability to respond to changes in the gradient direction, requiring negative feedback to counteract the spatial amplification.

Mathematical modelling of cell polarisation highlights the potential tradeoffs between all-or-none localisation of components to a narrow region and tracking of a moving signal source. Intuitively, positive feedback is required for amplification, but this feedback can impede the ability of the

cell to follow a shift in gradient direction because the polarisation becomes 'stuck' in one direction. For example, sensing the gradient signal results in a response that deposits a slight excess of the polarised species at the front. The species recruits more of itself in a positive feedback driven process. If the positive feedback is sufficiently strong, then this self-recruitment becomes self-sustaining regardless of the input gradient direction. Meinhardt [6] first highlighted this tradeoff between amplification and tracking, and others have further explored this issue [7, 8].

During mating, budding yeast cells secrete mating pheromones (e.g. α -factor) which induce their partner to form a projection towards the source. This process is mediated by heterotrimeric G-protein signalling which acts as the sensor; the peptide pheromone binds and activates the cognate G-protein-coupled receptor [9, 10]. Activated receptor stimulates the production of $G\alpha$ -GTP and free $G\beta\gamma$ from inactive heterotrimer. The cell polarity response is mediated by the small G-protein Cdc42 [11]. Cdc42 is activated by Cdc24, which is recruited to the membrane by $G\beta\gamma$. The $G\beta\gamma$ -Cdc24 interaction connects heterotrimeric G-protein signalling to Cdc42 in cell polarity. Active Cdc42 orchestrates morphological changes including the assembly and positioning of the polarisome, and formation of the mating projection [12].

The most well-studied pheromone-induced morphology in yeast is the single mating projection. However, extended α -factor treatment (>2 h) results in the appearance of multiple mating projections that are created in a periodic manner [13]. In addition, the concentration of α -factor determines whether the projection is broad and can bend in the direction of the gradient or is thin and does not bend (straight) [14]. Finally, investigators have isolated a variety of polarity mutants that can give rise to abnormal projection morphologies [15, 16]. Thus, both wild-type and mutant yeast cells exposed to mating pheromone can produce diverse morphological behaviours.

Much of the recent mathematical modelling of yeast has been performed using non-spatial models [17]. Among the spatial models, the primary focus has been modelling the formation of a single polarisation site [18]. In more recent work, we examined the ability of yeast cells to form a second projection in response to a directional change in the gradient [8]. The literature on how different morphologies and cell shapes can arise in higher eukaryotic cells has concentrated on cytoskeletal dynamics [19]; there has been less attention on alternative adaptive polarity behaviours.

In this paper, we investigated the basis of this morphological plasticity through mathematical modelling. The basic model structure consisted of two stages (modules), and we explored different combinations of positive and negative feedbacks in each stage and how these feedback structures would affect the amplification/tracking tradeoff. Interestingly, the models gave rise to a range of cell polarity behaviours when we explored model structure and parameter space. In addition, we used a mechanistic model of yeast cell polarity to tie the simulations more closely to our previously reported experiments [20]. More specifically, we simulated a bending projection for the first time, investigated the role of polarised negative feedback during double projection formation, characterised how the combination of positive and negative feedbacks can generate periodic projection formation (a type of spatial oscillations), described how noise-induced periodic projections in the system could arise, used simulations of the mechanistic model and experiments to show the polarised distribution of receptor during projection bending, and reproduced the polarity phenotypes when the concentration of the scaffold protein Bem1 was varied. In summary, the combination of modelling and experiments furnished insights into the mechanistic basis for the diversity of pheromone-induced cell morphologies.

2 Results

2.1 Balancing spatial amplification and tracking by modulating positive and negative feedbacks in a two-stage model

Cells in a chemical gradient sense the gradient direction and respond by polarising components to a specific region, that is, front. This ability to transform a shallow external gradient into a steep (e.g. all-or-none) internal gradient we term 'spatial amplification' [8, 21]. If the chemical gradient changes orientation, then the cell will repolarise to follow the new direction, a process we refer to as 'spatial tracking' (Fig. 1a). In this section, we used simulations of simple generic models to analyse these two cell behaviours in terms of specific model features such as the number of

stages (modules) and the arrangement and strength of positive and negative feedback loops (Fig. 1b).

To make conclusions about polarisation (spatial amplification), we calculated the degree of localisation of the species after the application of an initial gradient. In the simulations, this polarisation is indicated by the height (and narrowness) of the peak at the front. To make conclusions about tracking, we changed the direction of the gradient (i.e. 180°) and examined whether the polarisation peak would move and re-align with the new gradient. If the polarisation stayed in the original location aligned with the former (initial) gradient direction, then it did not track. The different spatial dynamics of the polarisation, whether a single static site, a single site that moves (continuously or discontinuously) after a gradient switch, two sites or multiple sites that appear and disappear in periodic fashion can be interpreted as different cell morphologies which we describe in greater detail below.

Previously, we used mathematical modelling to investigate the potential tradeoffs between spatial amplification and tracking. We performed simulations on a single-stage generic model [8] in which the variable a represents a membrane-localised species that becomes polarised through an input-dependent Hill function (k_0 -term) and a positive feedback Hill function (k_1 -term)

$$\frac{\partial a}{\partial t} = D\nabla_s^2 a + \frac{k_0}{1+u^{-q}} + \frac{k_1}{1+(ap)^{-h}} - (k_2 + k_3 b)a \quad (1)$$

$$\frac{\partial b}{\partial t} = k_4(\bar{a} - a_{ss})b \quad (2)$$

$$p = 1 \text{ or } p = \frac{1}{1+u^{-q}}, \quad \bar{a} = \frac{\int_S a \, ds}{\int_S ds}$$

In this equation, u represents the input (i.e. chemical gradient), b is a negative feedback variable and q and h are Hill cooperativity constants. The integral negative feedback (2) sets the spatial average of a , and at steady-state $\bar{a} = a_{ss} = 1$. The function p is either 1 or it is an input-dependent Hill-term. Diffusion is on the membrane surface. The term $-k_2 a$ represents first-order removal (e.g. dissociation from the membrane) of the species a .

High positive feedback (large k_1 and h) produced the amplification necessary for strong polarisation, but this positive feedback also created hysteresis and multiple steady-states (multi-stability), thus preventing tracking because polarisation was not reversible and became 'stuck' at one end [8]. Indeed in one-stage simulations, there was a tradeoff between amplification and tracking. With high positive feedback (Fig. 1c, top left), the polarisation was amplified, but could not track a 180° shift in gradient direction. Low or no positive feedback resulted in reduced amplification, but the components readily tracked the directional change (Fig. 1c, top right). In previous work [22], we demonstrated that this tradeoff depended on the strength of the positive feedback, and used a combination of analysis (for a two-compartment system) and exhaustive simulation (for a continuous system) to show that this tradeoff could not be overcome for this particular model.

The first question is whether having two stages instead of one could ameliorate this tradeoff. The biological motivation is that the relevant cell polarity system in yeast contains two cascaded G-protein signalling pathways: heterotrimeric G-protein and Cdc42. From a systems

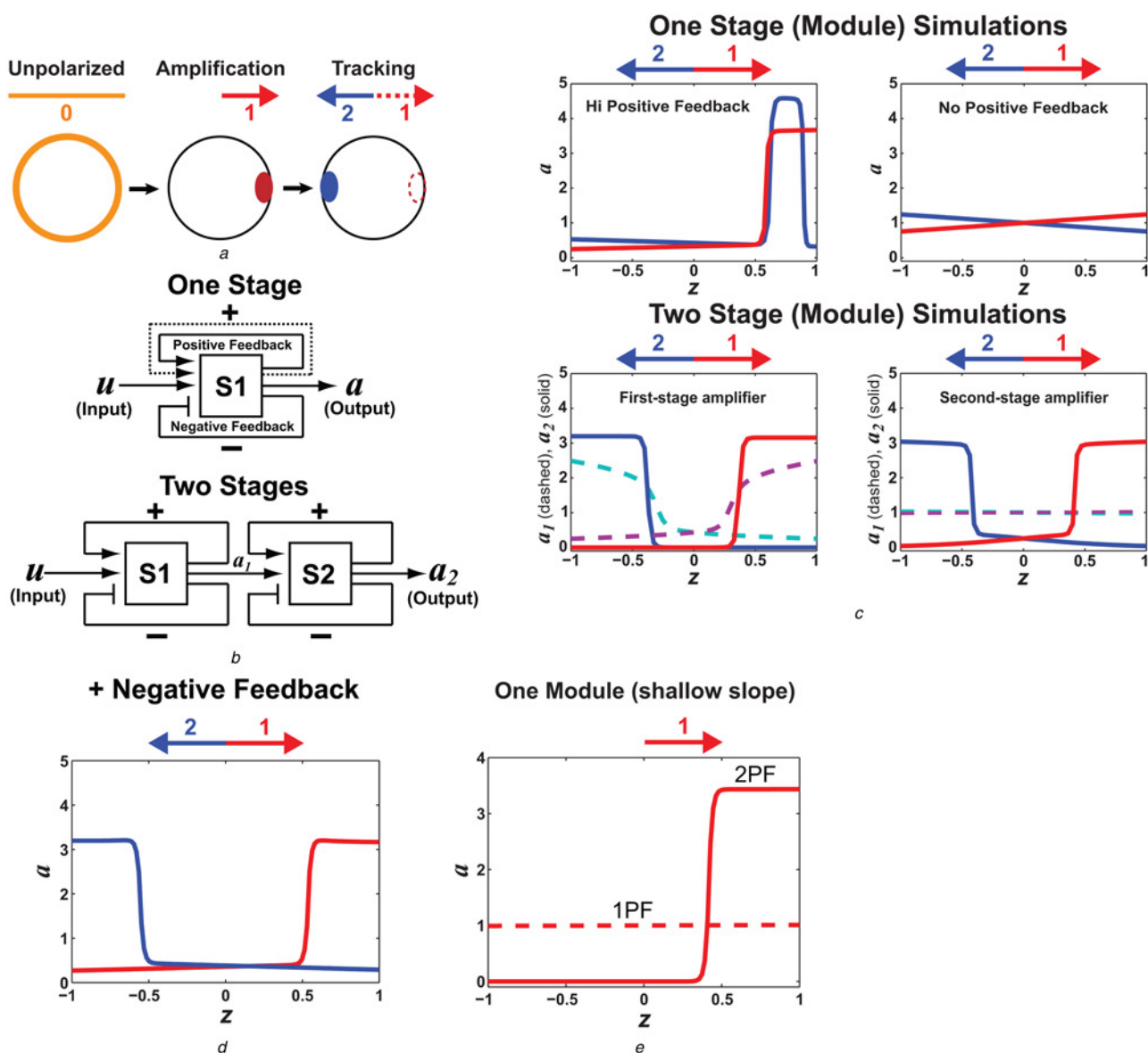


Fig. 1 Spatial amplification and tracking in one- or two-stage models containing different arrangements of positive and negative feedbacks

a Schematic diagram of spatial amplification and tracking

In spatial amplification, an isotropic component (0) becomes tightly localised (1) in response to an external gradient (arrow). In spatial tracking, the polarised component follows a change in the gradient direction (2).

b Schematic of one- or two-stage models with positive and negative feedbacks (denoted by + and -, respectively)

Each stage may possess more than one positive feedback loop (solid and dashed lines, top). Two-stage model is a cascade in which the output of stage 1 (S1) is the input to stage 2 (S2).

c Simulations (1D) of one-stage and two-stage models of cell polarity

Steady-state value of the polarisation variable (a , a_1 or a_2) is plotted against the axial length z . Top row shows one-stage simulations with high positive feedback (top left) and no positive feedback (top right). Response to the initial gradient and the response to the 180° switched gradient are shown. In the two-stage simulations (a_1 = module 1 output, dashed lines, and a_2 = module 2 output, solid lines), there were two scenarios: (i) the first module was the principal amplifier (bottom left) and (ii) the second module was the principal amplifier (bottom right).

d Polarised negative feedback facilitates tracking in the presence of strong positive feedback

1D simulations are from a one-stage model (a is plotted against z) which possesses high-positive feedback. Lines and gradient input are as described above in *c*. In the presence of polarised negative feedback, the model was able to track.

e Combination of two positive feedback loops increased spatial amplification

In a shallow gradient ($L_{slp} = 0.0001 \mu\text{m}^{-1}$), a single-stage model (a plotted against z) with one positive feedback loop (1PF, dashed line) was unable to create a polarised response. Two positive feedback model (2PF, solid line) produced substantial amplification and polarisation.

perspective, the additional stage provides an extra degree of freedom.

To this end, we constructed a two-stage model in which the output of the first module a_1 was the input to the second module whose output was a_2 (Fig. 1*b* and Section 2.1, Supplementary Material). In this model, it was possible to circumvent the tradeoff by splitting the amplification

between the two stages, and thus prevent multi-stability by reducing the positive feedback gain in a particular module. In one scenario, the amplification primarily arose from module 1 (Fig. 1*c*, bottom left); in the second scenario, there was strong positive feedback and amplification in module 2 (Fig. 1*c*, bottom right). In both cases, the combination of the two stages offered both good

amplification and good tracking. In a subsequent section, we interpret these results in the biological setting of heterotrimeric G-protein (stage 1) and Cdc42 (stage 2) signalling.

We examined a second strategy of using localised negative feedback to counteract the positive feedback generating the spatial amplification. In this manner, a single stage could employ greater positive feedback while still allowing tracking. The existing non-spatial integral negative feedback promotes stability by ensuring that $\bar{a} = 1$ at steady-state. We introduced a second polarised negative feedback loop that specifically neutralised the spatial amplification after a time-delay. Thus, the time constant for the polarised negative feedback has to be longer than the time constant for the initial polarisation. This additional feedback was implemented in the following model

$$\frac{\partial a}{\partial t} = D\nabla_s^2 a + \frac{k_0}{1+u^{-q}} + \left(\frac{k_1}{1+(\gamma ap)^{-h}} \right) \text{IF} - (k_2 + k_3 b + k_5 c) a \quad (3)$$

$$\frac{db}{dt} = k_4 (\bar{a} - a_{ss}) b \quad (4)$$

$$\frac{\partial c}{\partial t} = k_6 a - k_7 c \quad (5)$$

$$\text{IF} = \frac{1}{1+c^m}$$

The species c represents a negative regulator that is produced in response to a , and accumulates where levels of a are high. The inhibition factor term depends on c and down-regulates the positive feedback.

We started with a one-stage model with high positive feedback that was unable to track a directional change in the gradient (Fig. 1c, top left). Adding the polarised negative feedback allowed the initial polarisation to be suppressed so that a new site of polarisation could be created (Fig. 1d). Thus, the model could achieve high levels of polarisation with tracking. There was a new tradeoff, however, because the directional switch occurred only after the negative feedback suppressed the first polarisation site so that tracking was possible only after a time-delay.

Finally, we explored the implications of inserting a second positive feedback loop into a single module model. This modification was motivated by examples of systems possessing both an inner and an outer positive feedback loop [23]. Thus, instead of two positive feedback loops in series in two different modules, we combined two in parallel within the same module (Fig. 1b, top). We implemented this arrangement by replacing (1) in model 1 with (6)

$$\frac{\partial a}{\partial t} = D\nabla_s^2 a + \frac{k_0}{1+(ur)^{-q}} + \frac{k_1}{1+(ap)^{-h}} - (k_2 + k_3 b) a \quad (6)$$

$$r = \frac{a^s}{1+a^s}$$

The alteration to the model is that the k_0 -term now depends on a (via the Hill-term r with Hill constant s) creating positive feedback. In Fig. 1e, we found that the additional positive feedback loop increased the amplification so that at shallow

input gradient slopes, the two-loop, single-stage model was able to polarise (Fig. 1e, solid line), whereas the one-loop model could not (dashed line). The tracking properties of this architecture were also novel as we describe below.

In summary, two-stage models possessing multiple positive and negative feedback loops can generate a richer set of spatial dynamics and cell polarity behaviours than a one-stage model with a single positive feedback loop. We will attempt to characterise these behaviours in a more systematic fashion in the next section.

2.2 Modelling of mating morphologies using spatial compartments

One objective of this work is to provide a systematic investigation of the dynamics of the two-stage model with multiple feedbacks. For computational efficiency, we opted to start with a coarser spatial description using compartments instead of the finer grid of a partial differential equation (PDE) representation. In previous work, we used compartment models to investigate the multi-stability and loss of tracking that arose with higher positive feedback gains in a single-stage model with a single positive feedback loop and integral feedback control [22]. A schematic of the compartment model is shown in Fig. 2a. Here, we extended this approach to analyse more complex models, and identify a broader spectrum of dynamical behaviours. In Figure S1 (Supplementary Material), we explored the role of p in the positive feedback term ($k_1/(1+(ap)^{-h})$) which facilitates spatial tracking by making the positive feedback sensitive to the gradient direction.

In model 3, adding the second positive feedback loop to a single stage (6) enhanced amplification (Fig. 1e), but also created multi-stability and the loss of tracking (data not shown). However, one could restore tracking by reducing the gain in both positive feedback loops. Interestingly, the dynamics of this tracking was different from the single positive feedback loop system. These differences were more clearly seen in a three-compartment model, which adds a middle compartment to the two-compartment model. In the three-compartment description, during a directional change, the dual positive feedback model (2PF) exhibited an intermediate transition in which the middle compartment possessed the maximum polarisation. In contrast, the polarisation in the single positive feedback model (1PF) immediately switched from one end to the other (Fig. 2b) with no polarisation in the middle. Thus, there was a continuous shift in polarisation in the 2PF system compared with the discontinuous jump observed in the 1PF system.

Next, focusing on negative feedback, we implemented the compartment version of the polarised negative feedback model (model 2). This additional feedback loop possessed a spatial component that allowed it to counteract the positive feedback producing polarisation, whereas the integral control feedback was non-spatial and enhanced stability in the whole system by preventing the total amount of the species a from growing unbounded. An exploration of the parameter space of this model showed that increasing the strength of the negative feedback gain could suppress the polarisation. More interestingly, at high levels of negative feedback (and increasing time-delay) the system began to oscillate (Fig. 2c). Thus, the combination of positive feedback and polarised negative feedback produced oscillations.

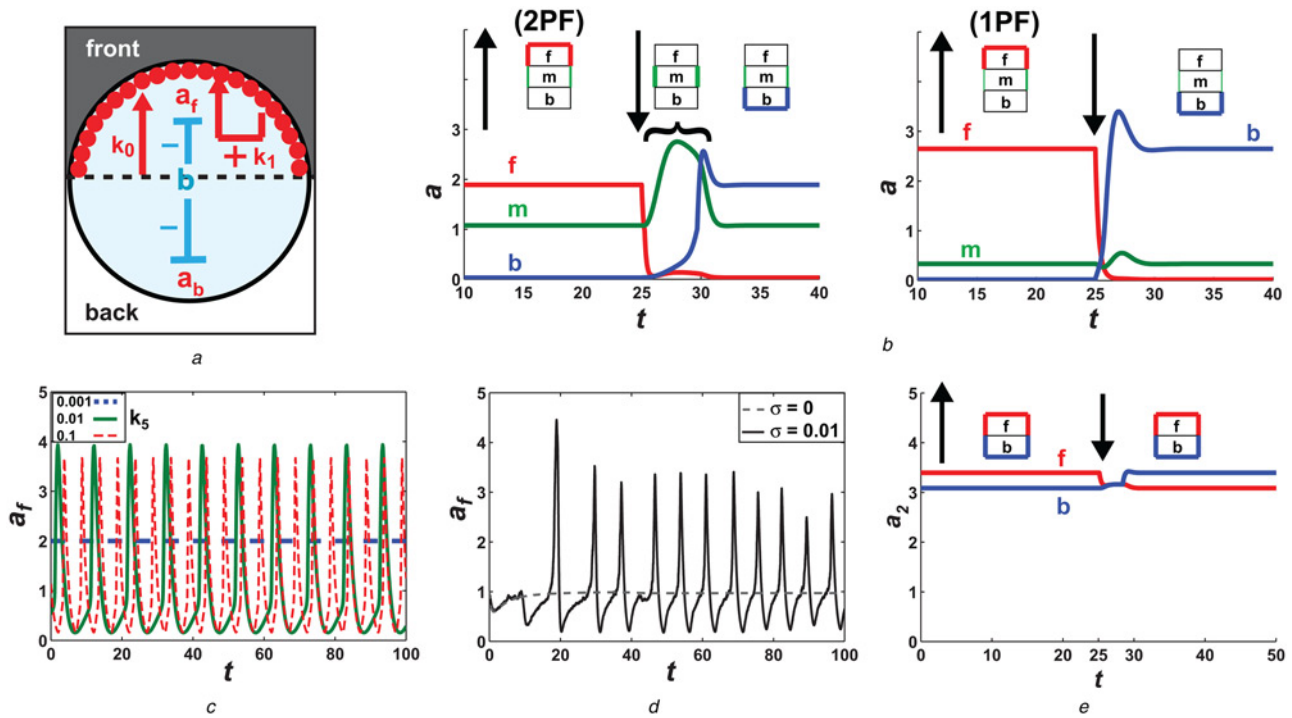


Fig. 2 Compartment modelling of mating morphologies

a Schematic diagram of two-compartment spatial model

Cell is divided in half into two compartments; a_f is the value of a in the front compartment and a_b is the value of a in the back compartment. Input gradient is indicated by the darker shading in the exterior of the front compartment. Polarised species a is represented by the circles on the perimeter of the circle. Polarisation of a is generated by an input-dependent Hill-term (k_0 -term) and by positive feedback (k_1 -term). Species b is a negative regulator of a .

b Continuous against discontinuous repolarisation in the three-compartment spatial description

Value of a in the front compartment with respect to the initial gradient is plotted (a_f). Direction of the external gradient is indicated by the black arrows and the gradient direction is switched at $t=25$. In the single-stage model, we compared dual (2PF) against single (1PF) positive feedback in a three-compartment representation. We plotted the concentration of a at the front (with respect to initial gradient), middle and back. Bracket shows the intermediate polarisation in the 2PF model during repolarisation that is absent in the 1PF model. In both models, the positive feedback gain was high in all modules ($k_{11}=k_{21}=10$, 2PF and $k_1=10$, 1PF).

c Time-delayed polarised negative feedback generates limit-cycle oscillations. In a single-stage model with polarised negative feedback (poINF), increasing the feedback gain resulted in sustained oscillations. The variable a_f is plotted over time as we increased the feedback gain from 0.001 to 0.1 [$k_5=0.001$ (dashed), 0.01 (solid), 0.1 (dashed)].

d Noise-induced oscillations in polarised negative feedback (poINF) model

At weaker negative feedback gains, there were no oscillations ($\sigma=0$, dashed). However, adding input noise ($\sigma=0.01$, solid) produced oscillations.

e Simultaneous polarisation in both compartments

In simulations of a two-stage model with proportional control instead of integral control and strong positive feedback in both stages, the value of the output of the system (a_2) was above two in both compartments after the directional change (a_{2f} and a_{2b}) representing dual polarisation.

When the strength of the negative feedback was reduced, there were no sustained limit-cycle oscillations. However, introducing noise into the input resulted in oscillatory behaviour (Fig. 2*d*). These dynamics are reminiscent of the noise-induced oscillations described by Vilar *et al.* [24]. Thus, depending on the negative feedback gain, there could be sustained oscillations or noise-induced oscillations in the compartment representation of the polarised negative feedback model.

Finally, we wished to explore modifications to the integral control loop; this feedback ensured that the total concentration of the species a is 1 at steady-state. We relaxed this constraint by replacing the integral control with proportional control [25] (see Section 2.4, Supplementary Material). From a control perspective, proportional control provides better regulation of transient disturbances, whereas integral control provides better steady-state regulation [25]. From a biological perspective, proportional control requires different dynamics in the feedback equation, and hence different dynamics for the key regulatory species. Interestingly, this alternative control scheme gave rise to a new behaviour in which both compartments contained

levels of a above 1 (Fig. 2*e*). We interpreted this response to be polarisation in both compartments.

In Table 1, we summarise the results from this section. Note the qualitatively different dynamical behaviours achieved with different combinations of parameters and model structures. We also show the correspondence between the behaviours and different cell morphologies.

2.3 Continuous space (PDE) modelling of mating morphologies

In this section, we extend our analysis of polarity behaviours observed in the compartment models to simulations using the finer spatial description of a PDE representation. We first explored models with two positive feedback loops in a single module (2PF). In Fig. 1*e*, we showed the amplification advantage of two loops against one positive feedback loop for a single parameter set. In Figure S2 (Supplementary Material), we show the amplification advantage over a range of parameter values for q .

Next, we examined the intermediate dynamics of the repolarisation in the two types of models (2PF against 1PF).

Table 1 Morphology table

Models	Parameters	Gradient	Dynamics	Morphology
1PF (first-stage standard)	$k_1 = \text{low}$ (low positive feedback)	initial	no amplification	no projection
1PF (first-stage standard)	$k_1 = \text{high}$ (high positive feedback)	initial	single amplification	initial projection
1PF–1PF (second-stage standard)	$k_{11} = \text{high}$ or $k_{21} = \text{high}$ (high positive feedback in one stage)	switch	discontinuous tracking	double projection
2PF–1PF (second-stage, 2PF in first-stage)	$k_{10} = \text{high}$, $k_{11} = \text{high}$ (dual positive feedback in first loops)	switch	continuous tracking	bending projection
1PF–1PF (second-stage standard)	$k_{11} = \text{high}$ and $k_{21} = \text{high}$ (high positive feedback in both stages)	switch	no tracking	single straight projection
1PF(polNF) (polarised negative feed)	$k_{\text{polNF}} = \text{high}$ (high negative feedback)	initial	limit-cycle oscillations	multiple projections
1PF(polNF) (polarised negative feed)	$k_{\text{polNF}} = \text{medium}$ (medium negative feedback)	noisy uniform	noise-induced oscillations	multiple projections
1PF(PC)–1PF(PC) (proportional control)	$k_{11} = \text{medium}$ and $k_{21} = \text{high}$ (positive feedback and proportional control)	switch	two amplifications	twin projections

Simulations from compartment models. The description of the parameters is in the Supplementary Material. Further description of the gradient, dynamics and morphology is in Fig. 4. For the models, 1PF = single positive feedback loop, 2PF = two positive feedback loops (in a single stage), 1PF–1PF represents a two-stage model with each stage containing one positive feedback loops and 1PF(polNF) is a stage containing polarised negative feedback. All of the models contained integral control, which is not explicitly denoted, except the model with proportional control, that is, 1PF(PC).

A three-compartment model showed that the additional feedback loop resulted in a continuous tracking behaviour (Fig. 2*b*). Indeed, in the PDE modelling, we found that with the second loop we observed continuous repolarisation through gradual movement of the polarised region (Fig. 3*a*). By contrast, in the 1PF model, we observed discontinuous jumping of the polarisation from the first site to the second. In a section below, we provide a mechanistic interpretation of the second ‘outer’ positive feedback loop as polarised transport of receptor so that input-sensing depends on polarisation of active G-protein.

In contrast to the compartment model, the PDE version of the strong polarised negative feedback model did not oscillate (data not shown); instead the cell could not generate a new site of polarisation after the first polarisation site was suppressed. However, in the presence of input noise, the system did oscillate. After the suppression of the initial polarisation, the system returned to a neutral state, and then the noise induced the second polarisation site (Fig. 3*b*). The new polarisation peaks appeared at random positions, but the timing (i.e. periodicity) depended on the model dynamics.

Finally, we tested the ability of the PDE version of the model to make simultaneous dual projections. As with the compartment model, we replaced the integral control with proportional control, and strengthened the positive feedback in the second stage. For specific parameter values, we were able to observe sustained polarisation at the first site in addition to a new second site when we switched the gradient direction (Fig. 3*c*). With integral control, we only observed a single peak.

2.4 Correspondence between computer simulations and biological morphological behaviours in yeast

We interpreted our results from the previous sections in terms of cell polarity behaviours. These behaviours included initial single projections, double projections, bending projections, single straight projections, oscillations and dual simultaneous projections (Fig. 4). The behaviours depended on the gradient conditions, as we previously showed experimentally [14, 20], as well as on the model structure and parameters.

In summary, the first part of the paper explored different types of polarised spatial dynamics using simplified models. In the second part of the paper, we apply the lessons we have learned to a mechanistic model of pheromone-induced yeast cell polarity.

2.5 Modelling continuous (bending projections) and discontinuous (second projections) repolarisation in the yeast mating G-protein system

In Figs. 2*b* and 3*a*, we demonstrated two different repolarisation behaviours: (i) continuous movement and (ii) discontinuous jumping of the polarisation region from the initial site to the final site. The first arose through the presence of an additional positive feedback loop that made sensing of the input gradient dependent on the polarisation variable.

In Fig. 1*c*, we outlined how a two-stage system can be superior to a one-stage system because the amplification can be split between the two stages, thus producing good amplification without the irreversibility (i.e. hysteresis from high positive feedback) that can impede tracking. In one strategy, the amplification was primarily in the first module; in the second strategy, the amplification was primarily in the second module. Previously, we constructed models of pheromone-induced yeast cell polarity that focused on the spatial dynamics of the heterotrimeric G-protein and the small G-protein Cdc42 [8, 26]. The first stage in the generic model can be thought of as the heterotrimeric G-protein system, and the second stage as the Cdc42 system. Details of the construction and validation of the model can be found in the Supplementary Material. Briefly the heterotrimeric G-protein part of the model was fit to detailed measurements of the system [27]. The Cdc42 part of the model was assigned parameter values from the literature and experimentally observed time constants [28]. Using the complete model, we were able to demonstrate qualitative and quantitative agreement to basic cell polarisation behaviours [8, 28, 29].

In Fig. 5*a*, we present a schematic diagram of the system. The input α -factor binds to α -factor receptor (Ste2) turning it on. Activated receptor stimulates the production of free $G\beta\gamma$ on the plasma membrane. Cdc24, which is recruited to the membrane by $G\beta\gamma$, activates the small G-protein Cdc42.

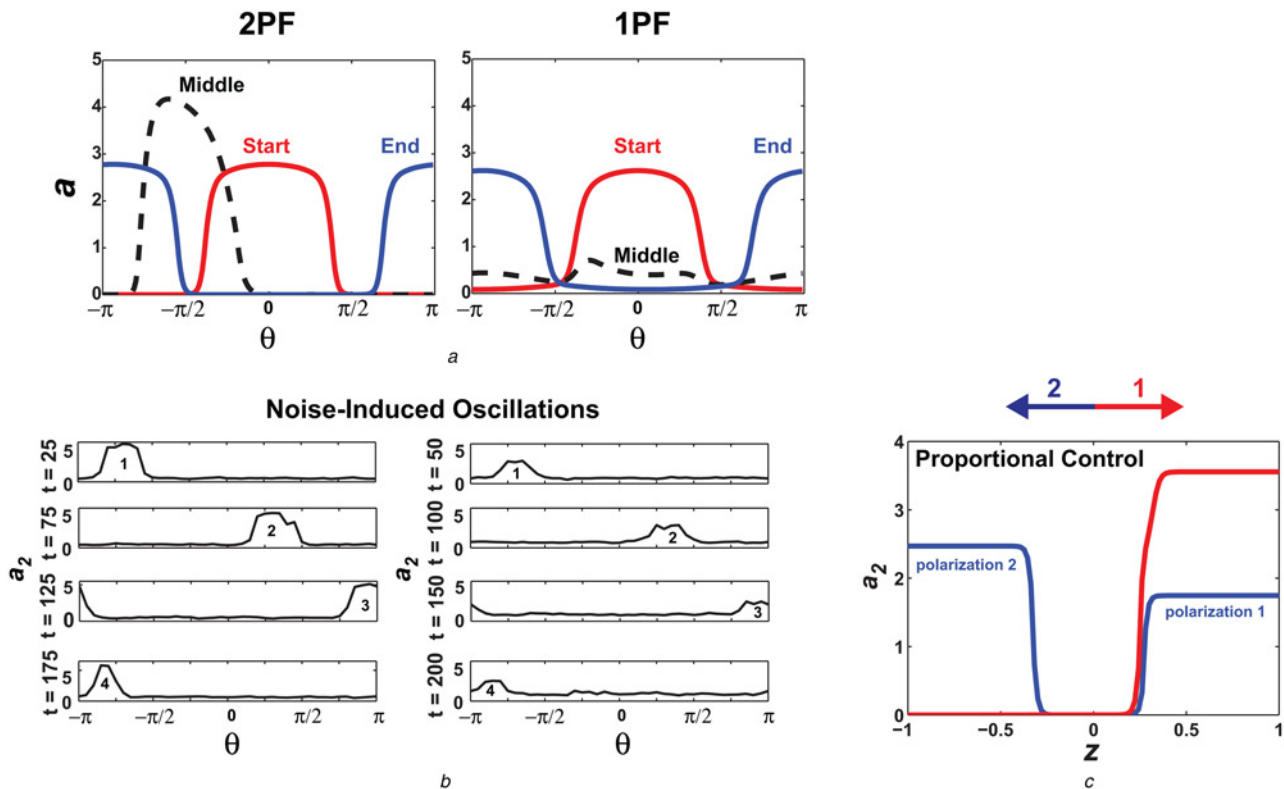


Fig. 3 PDE modelling of mating morphologies

a Presence of two positive feedback loops facilitates continuous repolarisation

Value of a is plotted against the radial position θ in 2D simulations of a single-stage model and left is the 2PF model and right is the 1PF model. We show the start ($t=0$), end ($t=100$) and middle time snapshots ($t \sim 50$, black dashed) of the simulations. 2PF model exhibits continuous repolarisation, whereas the 1PF model exhibits discontinuous jumping from the first to the second polarisation site.

b Noise-induced spatial oscillations in the PDE version of the two-stage model with polarised negative feedback

Oscillations were observed only in the presence of input noise. We plot snapshots of the 2D simulations at different time points from $t=25$ to $t=200$. Four polarisation sites are labelled 1–4 and show periodic appearance.

c PDE modelling of dual projection formation

We performed 1D simulations of the model containing proportional control and strong positive feedback in both modules ($k_{11}=k_{21}=10$). Value of a_2 (output of stage 2) is plotted against the axial length z . After reversing the direction of the gradient, the initial polarisation was maintained, while a second site of polarisation was created.

The scaffold protein Bem1 closes a positive feedback loop by binding to both active Cdc42 (Cdc42a) and Cdc24.

Experimentally, it has been observed that at low α -factor concentrations, the initial projection bends, and at high α -factor concentrations, second projections form [20]. Mutations that enhance heterotrimeric G-protein signalling favour projection bending, whereas mutations that enhance Cdc42 signalling favour the creation of double projections. Thus, there are two scenarios corresponding to bending projections and second projections, respectively.

We constructed a low α -factor cell polarity model (heterotrimeric G-protein dominant) and a high α -factor model (Cdc42 dominant). The key differences in the two models were manifested in the Cdc24 dynamics as shown below (see Supplementary Material Section 3.1 for more details about the model)

$$\begin{aligned} \frac{\partial[C24m]}{\partial t} = & D\nabla_s^2[C24m] + k_{24cm0}(Gbg_n^*)[C24c] \\ & + k_{24cm1}(B1^*)[C24c] - k_{24mc}[C24m] \\ & - k_{24d}[Cla4a][C24m] \end{aligned} \quad (7)$$

The variable C24 m represents Cdc24 on the membrane (where it can activate Cdc42), and C24c represents cytoplasmic Cdc24.

Note that the structure of (7) resembles the form of (1) of the generic model. This equation contains terms representing the cooperative recruitment of Cdc24 by $G\beta\gamma$ (the input to the second stage), positive feedback involving the scaffold protein Bem1 and first-order dissociation from the membrane. These reaction rates correspond to the k_0 , k_1 and k_2 terms, respectively, of the generic model (see Supplementary Material for more details).

In the low α -factor model, the ratio of the rate constants (k_{24cm0}/k_{24cm1}) (which corresponds to the ratio (k_0/k_1) in the generic model) was high; in the high α -factor model, this ratio was low emphasising positive feedback over input-sensing. In addition, in the high α -factor model, there was no polarised synthesis/transport of the receptor Ste2. In previous versions of the model [28, 29], we have examined both possibilities: (i) receptor is transported equally to all parts of the cell and (ii) receptor is transported to regions of the cell in which Cdc42 is active. In the low α -factor model, this polarised transport is represented by the term ($n_{C42a}k_{Rs}$), in which n_{C42a} represents normalised active Cdc42 and k_{Rs} is the Ste2 synthesis rate constant (see Eq. S7-1 in Section 3.1, Supplementary Material).

In the simulations, the initial gradient was run for 10 000 s (~ 3 h) and then the direction was switched from 0 to $(3\pi/4)$ for another 10 000 s. In the low α -factor model, the polarisation maintained the same front, but there was a

continuous shift in its position as the polarised active Cdc42 realigned with the new gradient direction (Fig. 5b). We interpreted this continuous repolarisation as a 'bending projection' with the front of the cell bending in the new direction. In the high α -factor simulations, the initial polarisation was inhibited after the input directional change, and then a new site of polarisation was created in the new gradient direction. We interpreted this discontinuous repolarisation as the formation of a second projection in the new direction. Thus, the two models could reproduce the two behaviours depending on whether the $G\beta\gamma$ term (heterotrimeric G-protein) was dominant or the Bem1 term (Cdc42 positive feedback) was dominant in the Cdc24 spatial dynamics, illustrating how the two behaviours can arise agreeing with experimental observation [20].

Another key difference between the two models was in the distribution of the receptor Ste2. The low α -factor model contained the polarised synthesis of Ste2 so that receptor preferentially localised to the front, resulting in a positive feedback loop increasing the level of active G-protein (active Ste2 \rightarrow $G\beta\gamma$ \rightarrow active Cdc42 \rightarrow polarised transport

of newly synthesised Ste2). Ste2 is part of the amplification mechanism through polarised transport and localisation to the projection. In the high α -factor model, receptor had to be more uniformly distributed on the cell surface including the cell body to allow for the sensing required for second projection formation when the gradient direction was switched (Fig. 5c).

Thus, one insight from the modelling was the expectation of a more localised appearance of receptor when the cell undergoes continuous repolarisation (low α -factor). When we imaged Ste2-GFP in a 0–100 nM gradient after 3 h, receptor was mainly found in the projection at low α -factor (Fig. 5d), whereas it was more evenly spread over the cell in high α -factor. (Fig. 5d). The data from a population of cells are shown in Figure S3 (Supplementary Material).

In summary, consistent with the results from the generic modelling, the key to the continuous repolarisation in the mechanistic model was that sensing of the input gradient depended on a variable that was polarised. In this case, the polarised species was receptor, which was transported specifically to the projection after synthesis resulting in an additional positive feedback loop.

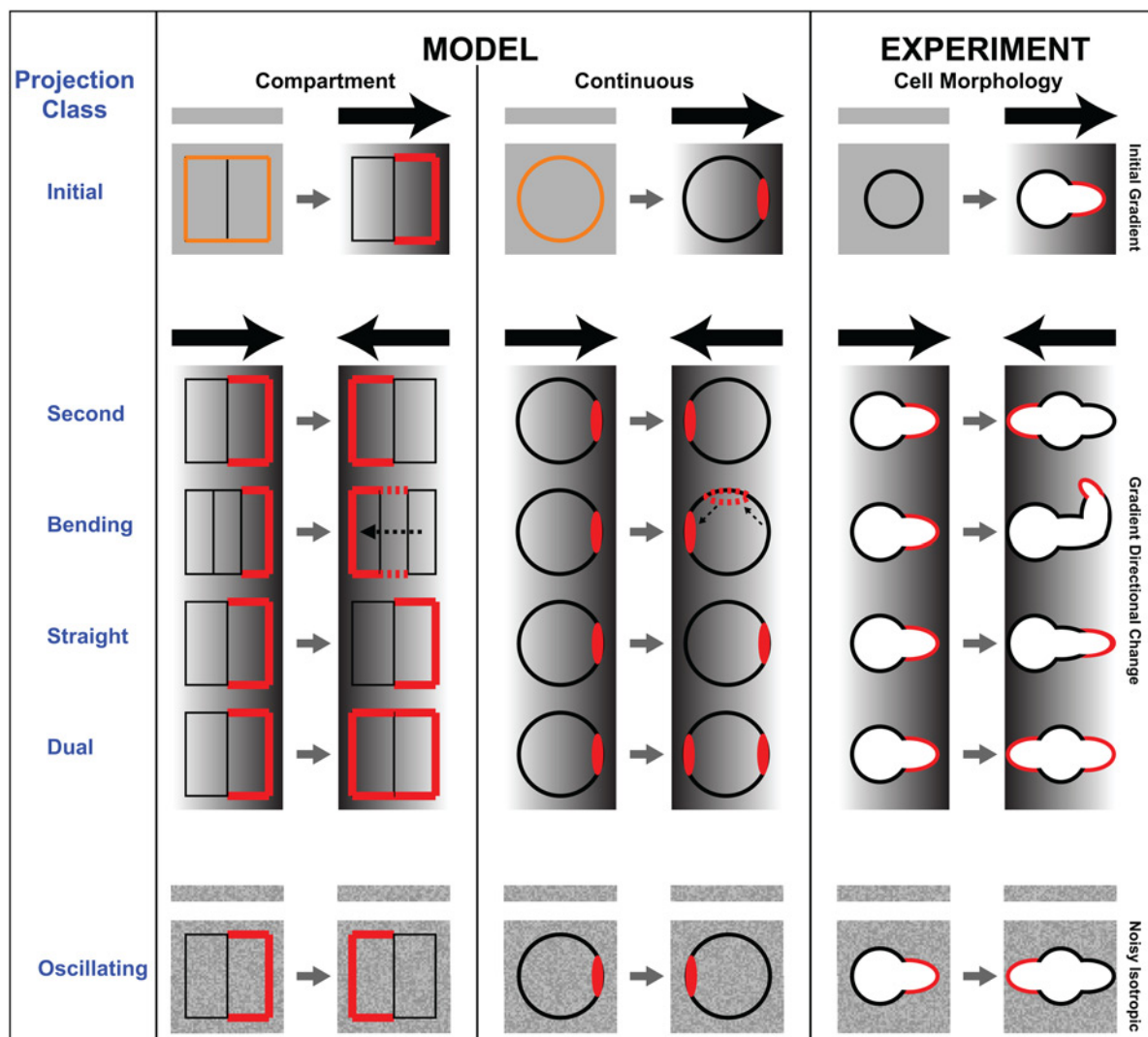


Fig. 4 Schematic diagram showing the relationship between computer simulations and pheromone-induced cell morphologies

There are three input conditions: (i) initial gradient (top), (ii) gradient switch (middle) and (iii) noisy isotropic (bottom). There are three columns: (i) compartment model, (ii) continuous model and (iii) cell morphology. Red/grey indicates the polarisation of a particular species in the simulations or in the cell. Rows represent different mating projection morphologies (projection classes) observed both computationally and experimentally. Note for the oscillating class (bottom), multiple projections appear in a periodic fashion in random directions.

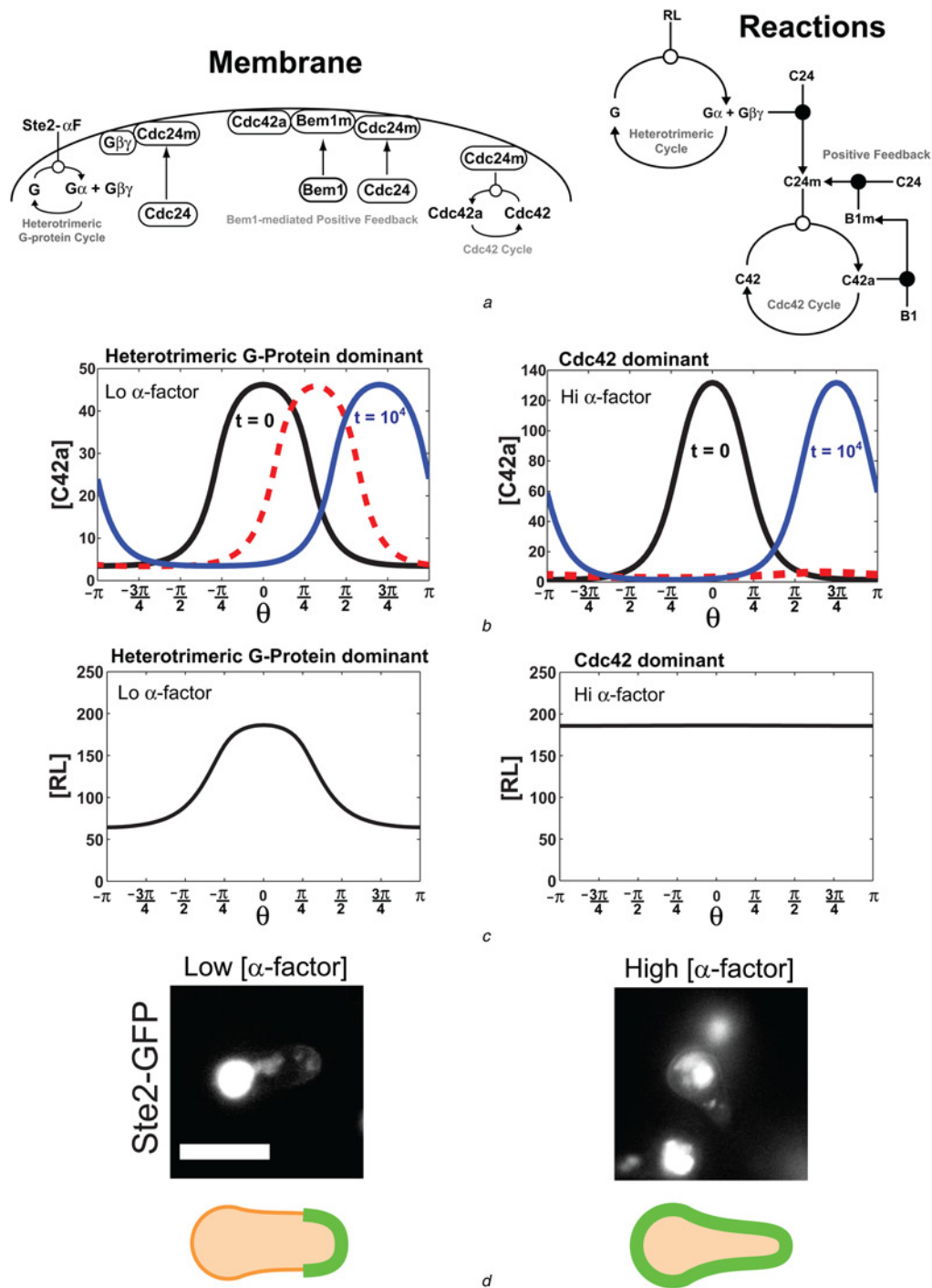


Fig. 5 Models of projection bending and second projection formation

a Schematic diagrams of pheromone-induced cell polarisation

Membrane diagram (left) shows localisation of key components to the plasma membrane initiated by activation of heterotrimeric G-protein leading to formation of free $G\beta\gamma$, and enhanced by the positive feedback loop involving Cdc24, Cdc42 and Bem1. Reaction diagram (right) shows the output of the heterotrimeric G-protein cycle ($G\beta\gamma$) feeding into the Cdc42 cycle which is amplified by the Bem1-mediated positive feedback loop. C24 = Cdc24, C42 = Cdc42, C42a = Cdc42a (activated Cdc42), B1 = Bem1, RL = receptor bound to ligand. Subscript *m* refers to the membrane-bound species. Open circles represent catalytic reactions, and the filled circles represent binding reactions.

b Simulations reproduced projection bending and second projection behaviours

In 2D simulations of the yeast cell using a mechanistic model of cell polarity, we plotted active Cdc42 (C42a, molecules/ μm^2) against the arc length θ . Initial gradient was at $\theta = 0$ and the final gradient was at $\theta = (3\pi/4)$; the polarisation response ($t = 0$ s) is represented by the solid black line, and the final polarisation response is the solid blue/grey line ($t = 10\,000$ s). Intermediate response is shown by the dashed line. Top graph is a simulation of the low α -factor model in which the heterotrimeric G-protein is dominant (see text). Bottom graph is a simulation of the high α -factor model in which Cdc42 is dominant.

c Simulations of receptor distribution at low (top) and high (bottom) α -factor

Receptor–ligand levels (molecules/ μm^2) are plotted against radial position. In the low α -factor model, receptor–ligand (RL, solid) shows a polarised distribution. In the high α -factor model, receptor–ligand is unpolarised.

d Ste2 localisation at low and high α -factor

Ste2-GFP was imaged in a 0–100 nM gradient after 3 h. At the low end of the gradient (low α -factor), Ste2 exhibited a polarised appearance with receptor localised at the front. At the high end of the gradient (high α -factor), Ste2 exhibited a more spatially uniform distribution over both the projection and cell body. Scale bar = 10 μm .

2.6 Overexpressing Bem1 and enhancing positive feedback in the Cdc42 module results in loss of tracking

The scaffold protein Bem1 (B1) forms a critical part of the primary positive feedback loop in the Cdc42 module involved in spatial amplification; it is recruited to the membrane (B1m) by active Cdc42 [C42a, (8)] where it binds and recruits Cdc24 [30] [$k_{24cm1}(B1^*)[C24c]$ term in (7)]

$$\frac{\partial[B1m]}{\partial t} = D\nabla_s^2[B1m] + k_{B1cm}[C42a][B1c] - k_{B1mc}[B1m] \quad (8)$$

Deletion of Bem1 ('bem1 Δ ') or the C-terminal truncation of Bem1 ('bem1-s1') results in poor polarisation during mating [30]. However, quantitative modelling and analysis of the directional sensing and polarisation phenotypes of Bem1 variants have not been performed.

We simulated low (30 molecules/cell), medium (3000 molecules/cell) and high (30 000 molecules/cell) levels of total Bem1 during a gradient shift (180° change in gradient direction). The changes in Bem1 concentration correspond to modulating the gain of the positive feedback loop (Cdc24–Cdc42a–Bem1). 'In silico', we found that at low

Bem1 levels, the polarisation was transient and weak (Fig. 6a, top). At medium (wild-type (WT)) levels, the cells in the simulations sensed the new direction and responded by making a new polarisation peak in the proper (opposite) direction that is, wild-type double projection behaviour. At high levels of Bem1, the polarisation did not sense a switch in the gradient direction, but instead persisted in the initial direction (Fig. 6a, bottom). Note the different Bem1 colour bar scale for the three sets of simulations.

We experimentally tested the model predictions by expressing Bem1 from the regulatable P_{Tet} promoter [31, 32]. When Bem1 was overexpressed approximately 5-fold, the phenotype of ' P_{TET} –BEM1' cells was that they formed primarily a single straight projection that did not sense the gradient switch (Fig. 6b, 10–100 nM to 100–10 nM). There were only a few cells containing double projections (~20%), and the single projections were straight so that the projection directional change after the gradient switch was $\Delta\theta = -2^\circ \pm 5^\circ$, which is close to 0, where $\Delta\theta$ represents the change in projection direction between 2.5 h (right before the gradient switch) and 5 h at the end of the experiment. In mutants in which a 'bem1-s1' loss-of-function mutation [30] was used (which approximates the low Bem1 phenotype), the cells did not form a mating projection, and instead were round with no stable polarisation region. At wild-type levels of Bem1, we observed the typical

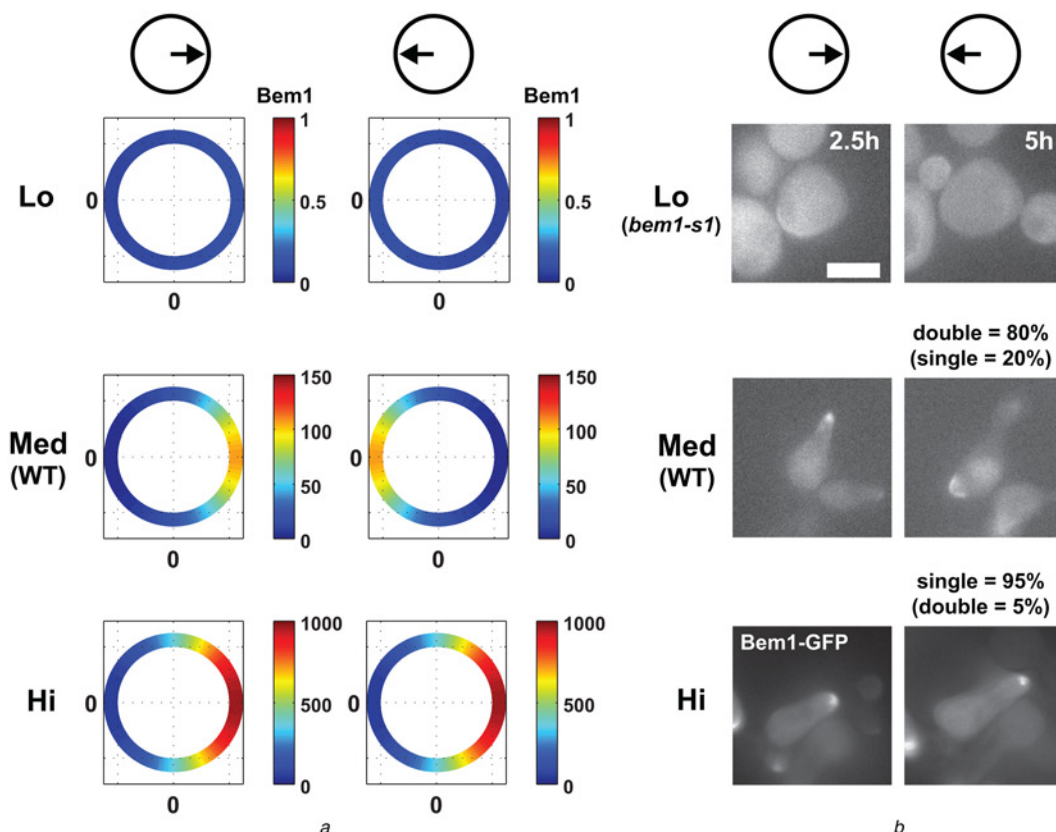


Fig. 6 Effects of varying the levels of Bem1 activity in simulations and experiments

a Simulations of polarisation behaviours at low, medium and high Bem1 levels

We performed gradient switch simulations (180° change in direction as indicated by arrow in circle at top). Bem1 levels (molecules/ μm^2) at the membrane are indicated by colour on the 2D disc (note different colour bar scales). We simulated low levels ($Bem1_{tot} = 30$), medium levels ($Bem1_{tot} = 3000$ molecules/cell) and high levels ($Bem1_{tot} = 30\,000$ molecules/cell), of total Bem1.

b Experimental results for varying the levels of Bem1 activity

Fluorescence imaging of cells containing Bem1–GFP in a gradient directional switch experiment (10–100 nM to 100–10 nM) at 2.5 h (right before the switch) and 5 h (2.5 h after the switch): (i) bem1-s1 loss-of-function mutant, (ii) wild-type and (iii) ' P_{Tet} –Bem1–GFP' strain overexpressing Bem1 (Bem1-OX). Cells containing the C-terminal truncation of Bem1 (labelled with GFP) did not show stable polarisation, and the cells were round. Wild-type cells typically formed double projections (80%). Majority of Bem1-OX cells possessed a single straight projection (95%). Scale bar = 5 μm .

behaviour with most cells forming second projections; the remaining cells that possessed a single projection underwent significant bending, $\Delta\theta = -52^\circ \pm 5^\circ$ in contrast to the straight projections of the Bem1 overexpression strain. Thus, the experimental data were consistent with the simulations: cells containing low Bem1 activity polarised poorly, wild-type Bem1 cells were able to sense the directional change and responded by making a second projection and Bem1 overexpressing cells made a single straight projection that did not respond to the gradient switch.

3 Discussion

In this paper, we used mathematical modelling to explore the space of possible cell polarity behaviours in yeast cells treated with mating pheromone. Moving beyond simple descriptions of a single static site of polarisation, we simulated bending projections, straight projections, periodic multiple projections and simultaneous dual projections. Generic modelling suggested that a two-stage system with variable strengths and arrangements of positive and negative feedbacks could give rise to this multiplicity of morphologies. The resulting changes in the spatial dynamics of the models corresponded to different polarity behaviours.

One important result is that the modelling predicts spatial oscillatory dynamics in the system resulting in the formation of multiple projections. The key feature that enables these oscillations is the presence of time-delayed, polarised negative feedback that counteracts the positive feedback generating projection formation. This time-delay may arise through dynamics not explicitly represented in our mechanistic models such as MAPK signalling leading to pheromone-induced gene expression [33]. Interestingly, although limit-cycle behaviour was observed in the compartment version of the models, the sustained oscillations were not observed in the PDE version. Instead, the PDE models required noise to drive the oscillations. Thus, the combination of input noise, positive feedback and polarised negative feedback produced this polarity behaviour. It will be interesting to investigate in the future whether such noise-induced oscillations [24] may underlie other types of oscillatory spatial dynamics [34].

These results were not restricted to the generic models; our mechanistic model of pheromone-induced yeast cell polarity was also able to exhibit a diversity of morphology behaviours. The model possessed a two-stage architecture with the first stage representing the heterotrimeric G-protein system, and the second stage representing the Cdc42 system. Multiple mechanistically motivated positive and negative feedback loops were included. Simulations using different parameter values produced bending and straight projections, and multiple projections.

This research represents an advance over previous versions of our cell polarity model. In terms of model structure, we have added two positive feedback loops in a single module, we have included polarised negative feedback, and we have explored the consequences of relaxing the integral feedback control constraint. In terms of model behaviours, we have simulated bending projection, oscillating multiple projections and dual simultaneous projections. Future models need to be able to reproduce these wild-type and mutant behaviours while fitting new data.

Finally, this work offers insights into specific biological mechanisms and their functional roles. First, the polarised

transport of receptor creates a second positive feedback loop that promotes the bending projection behaviour. Second, the scaffold protein Bem1 is necessary for the positive feedback amplification that underlies stable polarisation, and mutants that overexpress or underexpress the protein possess defective phenotypes.

In the future, we would like to explicitly model the shape of cells by using a moving boundary method we have previously described [35], and thereby simulate the mating projection in greater geometric detail. It is also important to investigate the impact of adding stochastic dynamics to this spatial system. Finally, we would like to extend the mechanistic model to include the mitogen-activated protein kinase (MAPK) pathway [33] and the spatial dynamics of the polarisome [36].

4 Materials and method

4.1 Yeast strains and cell culture

All yeast strains were derivatives of RJD863 (W303) or BY4741 (S288C). Genetic techniques were performed according to standard methods [37]. Complete strain details are presented in Table S1 (Supplementary Material). Cells were cultured in yeast extract-peptone-dextrose media (YPAD media supplemented with adenine).

4.2 Image acquisition and analysis

Images were collected at 15 min intervals using a charge-coupled device (CCD) camera (Hamamatsu orca-2) connected to the Nikon inverted microscope equipped with an automated stage and controlled by the Metamorph software package (Molecular Devices) as described previously [14].

4.3 Simulations

The compartment model simulations were performed using a standard ordinary differential equation (ODE) solver in MATLAB. Membrane species were divided into two or three compartments; cytoplasmic species were placed into a separate compartment with access to all membrane compartments.

The PDE simulations were carried out on an axisymmetric surface in three-dimensional (3D) space or in the 2D space, in which the cell surface is a curve as previously described [8].

Numerical discretisations of each variable on the cell membrane were carried out in the arclength parameterisation variable α for both 1D and 2D simulations. All spatial derivatives in the equations were approximated using a second-order finite difference discretisation.

In a typical simulation, the number of grid points in space was 200 with a time-step of 5×10^{-4} s. We tested a range of grid and time-step sizes to assure convergence of the simulations. The simulations in this paper were well-resolved with the above discretisation.

4.4 PDE simulations and noise model

The external noise is assumed to be spatially uncorrelated, and so noise at each spatial point was generated by selecting independent and identically distributed stationary random variables at a given time-step [29]. We used a normal distribution with mean 0 and standard deviation σ .

4.5 Mathematical models

The generic models [8] and yeast mechanistic models [28, 29] have been described previously. More details are provided in the Supplementary Material section.

5 Acknowledgments

We acknowledge discussions with members of the Nie and Yi labs as well as with the systems biology community at UCI. This research was funded by the NIH grants R01GM75309 and P50GM76516, and NSF grants DMS0917492 and DMS1161621. TIM was partially supported by the NIH Training Grant in Systems Developmental Biology HD060555-01. CSC is supported by the NSF DMS1020625. TMY is supported by the NSF DMS1001006.

6 References

- Drubin, D.G., Nelson, W.J.: 'Origins of cell polarity', *Cell*, 1996, **84**, (3), pp. 335–344
- Lumsden, A.G., Davies, A.M.: 'Earliest sensory nerve fibres are guided to peripheral targets by attractants other than nerve growth factor', *Nature*, 1983–1984, **306**, (5945), pp. 786–788
- Singer, S.J., Kupfer, A.: 'The directed migration of eukaryotic cells', *Annu. Rev. Cell Biol.*, 1986, **2**, pp. 337–365
- Devreotes, P.N., Zigmond, S.H.: 'Chemotaxis in eukaryotic cells: a focus on leukocytes and Dictyostelium', *Annu. Rev. Cell Biol.*, 1988, **4**, pp. 649–686
- Jackson, C.L., Hartwell, L.H.: 'Courtship in *S. cerevisiae*: both cell types choose mating partners by responding to the strongest pheromone signal', *Cell*, 1990, **63**, (5), pp. 1039–1051
- Meinhardt, H.: 'Orientation of chemotactic cells and growth cones: models and mechanisms', *J. Cell Sci.*, 1999, **112**, pp. 2867–2874
- Iglesias, P.A., Devreotes, P.N.: 'Navigating through models of chemotaxis', *Curr. Opin. Cell Biol.*, 2008, **20**, (1), pp. 35–40
- Chou, C.-S., Nie, Q., Yi, T.-M.: 'Modeling robustness tradeoffs in yeast cell polarization induced by spatial gradients', *PLoS One*, 2008, **3**, (9), p. e3103
- Sprague, G.F.J., Thorner, J.W.: 'Pheromone response and signal transduction during the mating process of *saccharomyces cerevisiae*. The molecular and cellular biology of the yeast *saccharomyces*: gene expression' (Cold Spring Harbor Laboratory Press, 1992), pp. 657–744
- Dohlman, H.G., Thorner, J.W.: 'Regulation of G protein-initiated signal transduction in yeast: paradigms and principles', *Annu. Rev. Biochem.*, 2001, **70**, pp. 703–754
- Pruyne, D., Bretscher, A.: 'Polarization of cell growth in yeast: I. establishment and maintenance of polarity states', *J. Cell Sci.*, 2000, **113**, pp. 365–375
- Pruyne, D., Bretscher, A.: 'Polarization of cell growth in yeast: II. the role of the cortical actin cytoskeleton', *J. Cell Sci.*, 2000, **113**, pp. 571–585
- Bidlingmaier, S., Snyder, M.: 'Regulation of polarized growth initiation and termination cycles by the polarisome and Cdc42 regulators', *J. Cell Biol.*, 2004, **164**, (2), pp. 207–218
- Moore, T.I., Chou, C.S., Nie, Q., Jeon, N.L., Yi, T.M.: 'Robust spatial sensing of mating pheromone gradients by yeast cells', *PLoS One*, 2008, **3**, (12), p. e3865
- Arkowitz, R.A., Lowe, N.: 'A small conserved domain in the yeast Spa2p is necessary and sufficient for its polarized location', *J. Cell Biol.*, 1997, **138**, pp. 17–36
- Evangelista, M., Blundell, K., Longtine, M.S., *et al.*: 'Bni1p, a yeast forming linking cdc42p and the actin cytoskeleton during polarized morphogenesis', *Science*, 1997, **276**, (5309), pp. 118–122
- Kofahl, B., Klipp, E.: 'Modelling the dynamics of the yeast pheromone pathway', *Yeast*, 2004, **21**, (10), pp. 831–850
- Layton, A.T., Savage, N.S., Howell, A.S., Carroll, S.Y., Drubin, D.G., Lew, D.J.: 'Modeling vesicle traffic reveals unexpected consequences for Cdc42p-mediated polarity establishment', *Curr. Biol.*, 2011, **21**, pp. 184–194
- Ofer, N., Mogilner, A., Keren, K.: 'Actin disassembly clock determines shape and speed of lamellipodial fragments', *Proc. Natl. Acad. Sci. USA*, 2011, **108**, pp. 20394–20399
- Moore, T.I., Tanaka, H., Kim, H.J., Jeon, N.L., Yi, T.-M.: 'Yeast G-proteins mediate directional sensing and polarization behaviors in response to changes in pheromone gradient direction', *Mol. Biol. Cell*, 2013, **24**, pp. 521–534
- Dawes, A.T., Edelstein-Keshet, L.: 'Phosphoinositides and Rho proteins spatially regulate actin polymerization to initiate and maintain directed movement in a one-dimensional model of a motile cell', *Biophys. J.*, 2007, **92**, pp. 744–768
- Zheng, Z., Chou, C.-S., Yi, T.-M., Nie, Q.: 'Mathematical analysis of steady-state solutions in compartment and continuum models of cell polarization', *Math. Biosci. Eng.*, 2011, **8**, pp. 1135–1168
- Brandman, O.Jr., Ferrell, J.E., Li, R., Meyer, T.: 'Interlinked fast and slow positive feedback loops drive reliable cell decisions', *Science*, 2005, **310**, pp. 496–498
- Vilar, J., Kueh, H.Y., Barkai, N., Leibler, S.: 'Mechanisms of noise-resistance in genetic oscillators', *Proc. Natl. Acad. Sci. USA*, 2002, **99**, pp. 5988–5992
- Franklin, G.F., Powell, J.D., Emami-Naeini, A.: 'Feedback control of dynamic systems' (Addison-Wesley Publishing Company, Reading, MA, 1994, 3rd edn.)
- Andrews, B.W., Iglesias, P.A.: 'An information-theoretic characterization of the optimal gradient sensing response of cells', *PLoS Comput. Biol.*, 2007, **3**, (8), p. e153
- Yi, T.-M., Kitano, H., Simon, M.I.: 'A quantitative characterization of the yeast heterotrimeric G protein cycle', *Proc. Natl. Acad. Sci. USA*, 2003, **100**, (19), pp. 10764–10769
- Yi, T.-M., Chen, S., Chou, C.-S., Nie, Q.: 'Modeling yeast cell polarization induced by pheromone gradients', *J. Stat. Phys.*, 2007, **128**, pp. 193–207
- Chou, C.-S., Bardwell, L., Nie, Q., Yi, T.-M.: 'Noise filtering tradeoffs in spatial gradient sensing and cell polarization response', *BMC Syst. Biol.*, 2011, **5**, p. 196
- Butty, A.C., Perrinjacquet, N., Petit, A., *et al.*: 'A positive feedback loop stabilizes the guanine-nucleotide exchange factor Cdc24 at sites of polarization', *Embo J.*, 2002, **21**, (7), pp. 1565–1576
- Belli, G., Gari, E., Piedrafitra, L., Aldea, M., Herrero, E.: 'An activator/repressor dual system allows tight tetracycline-regulated gene expression in budding yeast', *Nucleic Acids Res.*, 1998, **26**, (4), pp. 942–947
- Gari, E., Piedrafitra, L., Aldea, M., Herrero, E.: 'A set of vectors with a tetracycline-regulatable promoter system for modulated gene expression in *Saccharomyces cerevisiae*', *Yeast*, 1997, **13**, (9), pp. 837–848
- Madhani, H.D., Fink, G.R.: 'The riddle of MAP kinase signaling specificity', *Trends Genetics*, 1998, **14**, (4), pp. 151–155
- Lenz, P., Søgaard-Andersen, L.: 'Temporal and spatial oscillations in bacteria', *Nat. Rev. Microbiol.*, 2011, **9**, pp. 565–577
- Chou, C.-S., Moore, T.I., Chang, S., Nie, Q., Yi, T.-M.: 'Signaling regulated endocytosis and exocytosis lead to mating pheromone concentration dependent morphologies in yeast', *FEBS Lett.*, 2012, **586**, pp. 4208–4214
- Lawson, M.J., Drawert, B., Khammash, M., Petzold, L., Yi, T.-M.: 'Stochastic spatial dynamics enables robust cell polarization and gradient sensing', *PLoS Comput. Biol.*, 2013, **9**, p. e1003139
- Guthrie, C., Fink, G.: 'Guide to yeast genetics and molecular biology', *Meth. Enzymol.*, 1991, **194**, pp. 1–863